Model tags: direct three-dimensional tracking of heart wall motion from tagged magnetic resonance images

Alistair A. Young*

Department of Anatomy with Radiology, Department of Physiology, Medicine and Health Science Campus, University of Auckland, Private Bag 92019, Auckland, New Zealand

Abstract
Although magnetic resonance tissue tagging is a useful tool for the non-invasive measurement of three-dimensional (3-D) heart wall motion, the clinical utility of current analysis techniques is limited by the prohibitively long time required for image analysis. A method was therefore developed for the reconstruction of 3-D heart wall motion directly from tagged magnetic resonance images, without prior identification of ventricular boundaries or tag stripe locations. The method utilized a finite-element model to describe the shape and motion of the heart. Initially, the model geometry was determined at the time of tag creation by fitting a small number of guide points which were placed interactively on the images. Model tags were then created within the model as material surfaces which defined the location of the magnetic tags. An objective function was derived to measure the degree of match between the model tags and the image stripes. The objective was minimized by allowing the model to deform directly under the influence of the images, utilizing an efficient method for calculating image-derived motion constraints. The model deformation could also be manipulated interactively by guide points. Experiments were performed using clinical images of a normal volunteer, as well as simulated images in which the true motion was specified. The root-mean-squared errors between the known and calculated displacement and strain for the simulated images were similar to those obtained using previous stripe-tracking and model-fitting methods. A significant improvement in analysis time was obtained for the normal volunteer and further improvements may allow the method to be applied in a 'real-time' clinical environment.

1. INTRODUCTION

Magnetic resonance (MR) tissue tagging is a useful clinical tool for the non-invasive measurement of heart wall motion (Zerhouni et al., 1988; Axel and Dougherty, 1989). Typically, multiple parallel tagging planes of magnetic saturation are created orthogonal to the image plane in a short time interval (5–12 ms) on detection of the R wave of the ECG. Often a grid of tag planes is created, whose intersection with the image plane gives rise to dark bands ('image stripes'),

1–2 mm in width and spaced 5–10 mm apart. The image stripes deform with the tissue and fade according to the time constant $T1$ (~800 ms in the myocardium). Figure 1 shows a midventricular short-axis slice at end diastole (ED) and end systole (ES). Techniques for stripe tracking and strain estimation have been developed and validated in both two dimensions (2-D) (Young et al., 1993; Kraitchman et al., 1995) and three dimensions (3-D) (Young et al., 1995). Recently, a number of clinical studies have used MR tagging to characterize regional left ventricular (LV) wall motion and deformation in normal and diseased hearts (Palmon et al., 1994; Young et al., 1994).

*Corresponding author
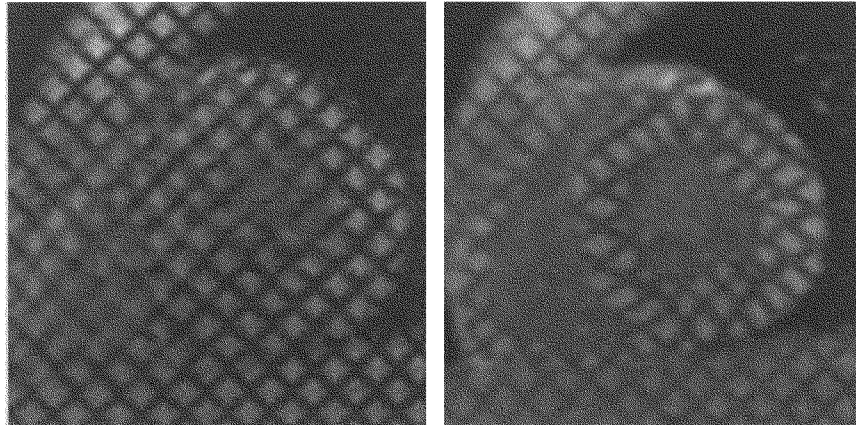(e-mail: a.young@auckland.ac.nz)

Figure 1. A midventricular short-axis slice at end diastole (left) and end systole (right), showing MR tagging stripes

The clinical utility of this technique is currently limited by the prohibitively long time required for image analysis. Most analysis methods require the prior extraction of the inner and outer boundaries of the LV in each image, together with the localization of the image tag stripes in each frame (O'Dell et al., 1995; O'Donnell et al., 1995, 1996; Young et al., 1995; Park et al., 1996a,b; Denney and McVeigh, 1997; Declerck et al., 1998). Several semi-automatic methods have been developed for tracking the tags and identifying the boundaries (Guttman et al., 1994; Young et al., 1995; Denney, 1997). However, the image intensity information is insufficient to completely characterize the boundary and tag locations, due to limited spatial and temporal resolution, lack of contrast between muscle and blood and respiration and gating artefacts. User interaction with the tracking and segmentation processes is therefore essential. As 3-D studies typically comprise more than 200 images (5–12 short-axis slices and 5–8 long-axis slices, each with 5–20 frames), the time required for user interaction can be substantial.

This paper describes a method for reconstructing regional LV motion and deformation directly from a set of long- and short-axis tagged MR images, without the need for separate boundary and tag tracking. Previous finite-element (FE) modelling techniques (Young et al., 1995, 1996) were extended to allow the model to deform directly under the influence of the images. A set of 'model tags' were embedded within the FE model, thereby defining a set of material surfaces which determined the location of the magnetic tag planes. Since the model tags deform with the FE model, intersections of the model tags with the image planes could be matched with the image stripes. User-derived constraints were imposed in the form of a small number of 'guide points', which could be used to manipulate the model. These were used to determine the initial geometry and establish

correspondence from frame to frame. The use of the 3-D model to track the image stripes simplified the image analysis problem since model tags were constrained to move in a coherent 3-D manner, allowing information from adjacent slices to influence the solution in any particular slice. User interaction was minimized since each guide constraint acted directly on the 3-D model. In addition, the 3-D myocardial deformation in any region of the heart can be calculated directly from the fitted model.

2. METHODS

2.1. Finite-element model
As done previously, a 16-element FE model was constructed to describe the geometry and motion of the LV (Young et al., 1994, 1995). Each element employed bicubic Hermite interpolation in the circumferential and longitudinal directions, with linear interpolation transmurally (Figure 2). Nodes shared position and derivative information between elements, giving C^1 continuity. Within each element, the geometric coordinate field x was given as a function of element or material coordinates ξ by a weighted average of nodal values:

$$\mathbf{x}(\xi_1, \xi_2, \xi_3) = \sum_n \Psi_n(\xi_1, \xi_2, \xi_3)\, \mathbf{x}^n \qquad (1)$$

where $\mathbf{x}^n$ are the nodal values and Ψ_n are the element basis functions. Note that the element coordinates ξ of material points do not change (by definition) as the model deforms.

Initially, the model was prescribed in a prolate spheroidal coordinate system (λ, μ, θ). Image fiducial markers were required to determine the initial position of the model with respect to the ED images. These were: (i) the location of the central axis at the centre of the LV in an apical short-axis
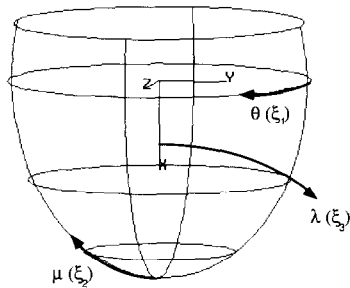
Figure 2. The 16-element model. (Outer surface only shown for clarity.) Element coordinates ξ_1, ξ_2, ξ_3 are in the circumferential, longitudinal and radial directions respectively. Rectangular Cartesian (x, y, z) and prolate spheroidal (λ, μ, θ) coordinate systems are also shown.

image; (ii) the location of the central axis at the LV in a basal short-axis image; (iii) the approximate centroid of the right ventricle (RV); (iv) a set of points around the basal margin of the LV muscle as seen in the long-axis images; (v) the location of the apex as seen in a long-axis image.

The origin was placed on the central axis of the LV one third of the distance from the base to the apex. Nodes were placed at equally spaced intervals in the two angular coordinates (μ, θ) and at a constant radial coordinate (λ). The centroid of the RV had $\theta = 0$ and the extent of the model in the μ direction was governed by the basal margin points. The distance from apex to base was used to determine the focal length of the prolate system and provided an overall scale factor for the LV.

2.2. Initial geometry

As a first step in the motion reconstruction problem, the approximate geometry of the LV at the time of tag creation (ED) must be determined. This was done interactively by manipulating a small number of guide points on the images. Due to the lack of blood/muscle contrast in tagged myocardial images, the endocardial contour is often difficult to determine. Image-derived constraints were therefore not employed for the geometry determination. In practice, the endocardial boundary cannot often be seen in the ED images because there has been insufficient time to wash out the tags in the blood pool. The geometry of a subsequent time frame (e.g. the second or third frame) was therefore determined first.

This was then deformed to the approximate ED position by displacing the guide points, using the relative motion of the tag stripes to indicate the guide point displacements.

To place a guide point, the user clicked on an image position and indicated the associated surface (epi- or endocardium). Each guide point was projected onto the model along lines of constant μ and θ and only the λ field was fitted by the linear least-squares method. Since there were far fewer guide points than model parameters, a smoothing term was added to the error function to minimize the first and second derivatives of the displacement field, as has been done previously (Terzopoulos, 1988). The error function minimized was therefore

$$E = S(\lambda) + \sum_g (\lambda(\xi_g) - \lambda_g)^2 \qquad (2)$$

where $S(\lambda)$ denotes the smoothing term, λ_g are the λ values for the guide points and $\lambda(\xi_g)$ denotes the λ values of the corresponding model points. The number of guide points employed must be sufficient to provide an approximate ED shape for input to the stripe-tracking algorithm. Only an approximate geometric description was required since boundary information was not used for the subsequent motion and deformation estimation.

Although the prolate spheroidal coordinate system is useful for representing the initial geometry, LV motion is not easily described in a polar system. The initial geometry was therefore converted to rectangular Cartesian 'cardiac coordinates' using the transformation

$$\begin{aligned} x &= f \cosh(\lambda) \cos(\mu) \\ y &= f \cosh(\lambda) \sin(\mu) \cos(\theta) \\ z &= f \sinh(\lambda) \sin(\mu) \sin(\theta) \end{aligned} \qquad (3)$$

where f is the focal length and x, y, z are the cardiac coordinates. The nodal values of the model were then given in cardiac coordinates and each coordinate field (x, y, z) was interpolated using bicubic Hermite/linear basis functions as in Equation (1).

2.3. Model tags

Image stripes arise from the intersection of tagged material surfaces with the image plane. They therefore provide some information about the underlying deformation of the heart but do not represent the motion of material points. Due to the tomographic nature of the imaging process, material points move through the fixed image slice planes during the deformation. This can result in the appearance and disappearance of image stripes from frame to frame due to the elliptical shape of the LV. In order to apply the correct image motion constraints to the model, a set of 'model tags'
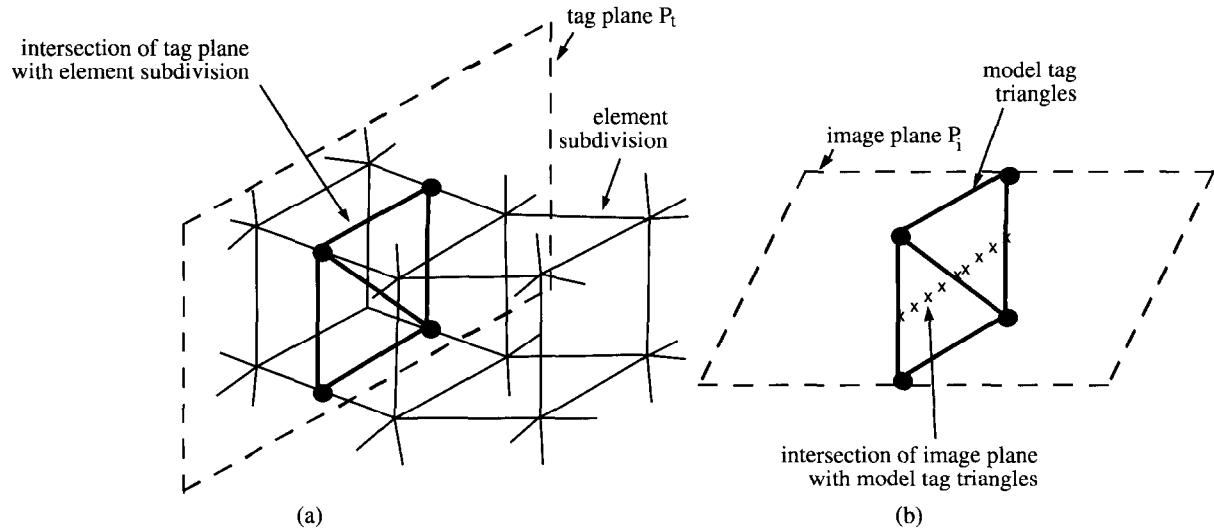
Figure 3. Calculation of model tags (**a**) and model stripe points (**b**). (a) Each model element is subdivided into small linear elements (thin lines). The tag planes P_t (dashed lines) are intersected with the element subdivision using a marching cubes algorithm. This results in a set of triangles (thick lines) which define the model tags. (b) Model tags (thick lines) are intersected with the image planes P_i (dashed lines) resulting in a set of model stripe points (x).

was created within the FE model. Model tags represent the material surfaces within the heart tissue which are tagged with magnetic saturation. They are required to define an image-based objective function which is used to deform the model to match the image stripes.

The location and orientation of the tag planes at the time of their creation (ED) were determined from the tagging pulse sequence parameters. Each tag plane P_t was described by a point on the plane p_t and a normal n_t to the plane. Similarly each image slice plane P_i was described by a point p_i and normal n_i. Each tag plane was associated with one or more image slice planes; let T_i denote the set of tag planes associated with each image plane P_i. Model tags were found using a subdivision algorithm (Lorensen and Cline, 1987; Young *et al.*, 1996), as follows. Each element was subdivided into N subelements with subelement nodes equally spaced in ξ-space. The tag planes were then intersected with the subelement mesh assuming a linear variation of ξ between subelement nodes. The result was a set of triangles whose vertices were given in element (material) coordinates. Figure 3a shows a schematic of this procedure. Since the vertices were stored in material coordinates, the location of the model tags was constant in (ξ_1, ξ_2, ξ_3)-space, whereas their physical location in (x, y, z)-space (cardiac coordinates) was determined by the nodal values x^n.

At any stage in the model-fitting and deformation process, a set of 'model stripe' points could be found by intersecting

the model tags with the image planes. For each model tag triangle which intersected the image plane, the intersecting edges were interpolated to result in a set model stripe points spaced ~ 1–2 mm apart (Figure 3b).

2.4. Model deformation

Let $M(i, t)$ denote the set of model stripe points associated with each $P_t \in T_i$. The model was deformed from frame to frame to minimize the following objective function:

$$E(\mathbf{x}) = S(\mathbf{x}) + \sum_{P_i} \sum_{P_t \in T_i} \sum_{j \in M(i,t)} w_j \left[\mathbf{n}_t \cdot (\mathbf{x}(\xi_j) - \mathbf{x}_j) \right]^2. \quad (4)$$

The first term is a smoothing constraint included to regularize the problem in the case of non-uniformly distributed data. The second term is an image displacement constraint which measures the match between model stripe points and image stripe points in the direction orthogonal to the tags: $\mathbf{x}(\xi_j)$ are the cardiac coordinates of each model stripe point $j \in M(i, t)$ and $\mathbf{x}_j$ are image stripe points associated with $\mathbf{x}(\xi_j)$. The w_j are weights derived from the image intensity function and $\mathbf{n}_t$ are the normals to the original tagging planes P_t. The dot product employed in Equation (4) is a statement of the aperture problem: image stripes provide information about displacement in the direction normal to the tag, whereas the position of the material point along the tag is unknown. This constraint is similar to displacement constraints used previously in optical flow problems (Hildreth, 1984).

The smoothing term measured the variation of the deformation from a prior geometry, as described previously (Young et al., 1995):

$$S(\mathbf{x}) = \int_\Omega \sum_k \left\| \frac{\partial F}{\partial \xi_k} \right\|_F^2 \partial\Omega \qquad (5)$$

where F is the deformation gradient tensor defined with respect to the rectangular Cartesian cardiac coordinate system and $\|\ \|_F^2$ is the Frobenius norm. The smoothing weights were set small enough to have negligible effects in regions containing sufficient data points. In regions with few or no data points, the effect of this smoothing term was to reduce the variation of deformation across the model (Young et al., 1995).

The error function Equation (4) was minimized using an iterative non-linear least-squares procedure [see the appendix and Young et al. (1996)]. In summary, each iteration consisted of the solution of Equation (4) by linear least squares (keeping the ξ_j constant), and the model stripe points $\mathbf{x}(\xi_j)$ were recalculated before the next iteration, along with their associated image stripe points $\mathbf{x}_j$.

2.5. Image stripe points

Image stripe points were associated with each model stripe point by searching the image in a small neighbourhood for the most likely point on the image toward which the model stripe point should displace. For each pixel, a likelihood function was defined to measure the probability that the pixel is located on the centre of an image stripe. The likelihood function was given by the output of stripe detection filters (one for each stripe orientation) convolved with the image. The stripe detection filters had a Gaussian shape in the direction parallel to the stripe and a second derivative of a Gaussian in the direction normal to the stripe (see Figure 4). The scale of the filter was tuned to the width of the tag stripes (in this paper all filters had $\sigma = 1.5$ pixels). The search was carried out in a small one-dimensional (1-D) neighbourhood centred about each model stripe point consisting of only those pixels in the direction orthogonal to the original tag plane and less than half the inter-stripe spacing from the model stripe point.

Rather than take the image point with the maximum filtered image value, the centroid (or centre of mass) of the 1-D neighbourhood was used as the image stripe point. The centroid was calculated as the average of all the points in the neighbourhood weighted by their filtered image values. This was a more robust measure of the position of the stripe centre than the maximum filtered value, and allowed the calculation of the image stripe centre to subpixel resolution. Centre-of-mass image constraints have previously been employed for active contour models and are more stable than gradient-based image constraints (Davatzikos and Prince, 1995, 1996). Finally, the weight w_j for each image stripe point was calculated to give a measure of the confidence of the image displacement constraint and was given by the maximum value of the filtered image in the neighbourhood. Myocardial pixels with low weight were therefore located either between stripes (where the search neighbourhood did not include a stripe centre) or on stripes running in the other direction.

Previous studies have shown that image stripe orientations do not change substantially during the cardiac cycle (typically $<20°$). The search direction was therefore kept constant throughout the tracking process (orthogonal to the original stripes). This enabled the result of the search to be precalculated before the stripe-tracking process. For each image, a displacement image was generated which stored the displacement from each pixel to the centroid of the filtered image in the search neighbourhood. To maintain subpixel resolution, the displacement was multiplied by a scaling factor before being stored as a 1 byte/pixel image. The weight for each pixel was similarly precalculated as an image. Figure 4 shows an example of a short-axis image at ES, showing raw, filtered, displacement and weighting images. The precalculated displacement and weighting images allowed fast calculation of the image displacement constraints: for each model stripe point the displacement to the associated image stripe point together with the associated weighting was given by a simple look-up operation.

2.6. User interaction

It is not uncommon for regions of the LV to move more than one stripe spacing between frames. User interaction was therefore required in order to bring the model into approximate correspondence with the image stripes (i.e. within range of the image displacement constraints). A fit to guide points was performed by minimizing Equation (4) above with a small number of guide points in place of the image stripe points:

$$E(\mathbf{x}) = S(\mathbf{x}) + \sum_g \sum_{P_{t(g)}} w_g \left[\mathbf{n}_t \cdot (\mathbf{x}(\xi_g) - \mathbf{x}_g) \right]^2 \qquad (6)$$

where each guide point $\mathbf{x}_g$ is associated with one model stripe point $\mathbf{x}(\xi_g)$ on the tag plane $P_{t(g)}$ corresponding to the guide point g. The smoothing term was the same as Equation (5) and ensured a smooth interpolation between guide point displacements. To define a guide displacement the user clicked on an image point to locate the guide point and then clicked on a model stripe point to define the associated model tag. At each iteration of the minimization of Equation (6), the $\mathbf{x}(\xi_g)$ were recalculated as the model stripe point closest to $\mathbf{x}_g$ on the corresponding tag plane $P_{t(g)}$. After these 'guide
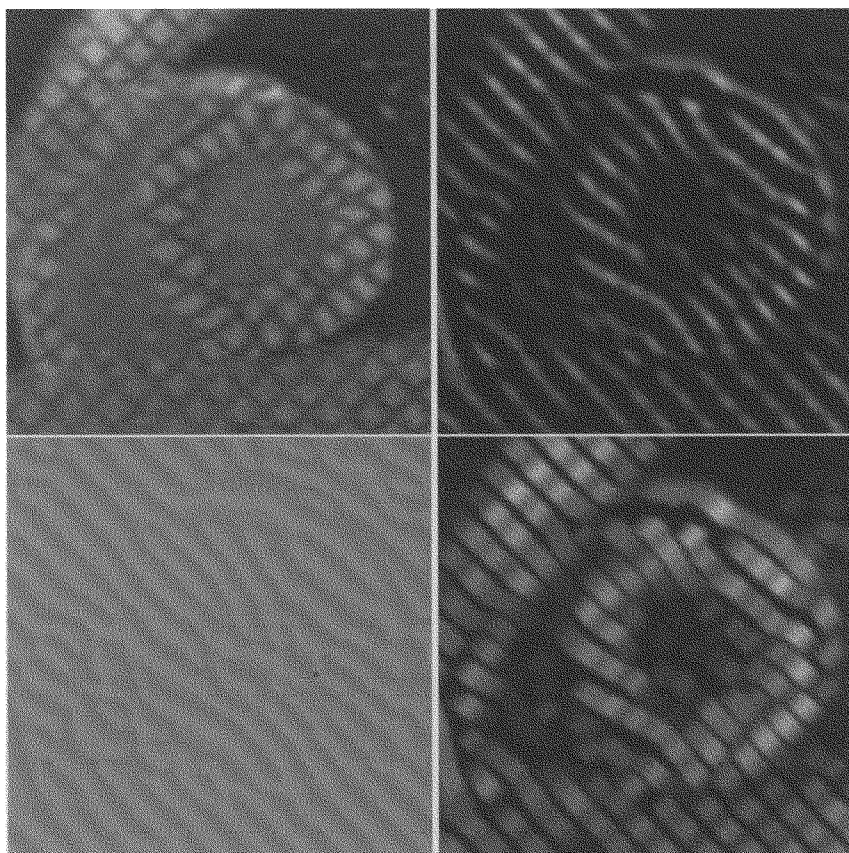
Figure 4. Precalculation of image displacement constraints as images. Top left, raw image; top right, result of the stripe detection filter in one orientation; bottom left, displacement image (lighter grey levels indicate displacement towards the top right, darker grey levels indicate displacement in the opposite direction); bottom right, weight image (lighter grey levels indicate higher weighting).

iterations' the model stripe points should be within range of the image displacement constraints and the fit could proceed with 'image iterations' as in Equation (4). The user was also able to interact with the image iteration by selecting a group of model stripe points and redefining their associated image stripe points.

2.7. Image acquisition

In vivo clinical images of a normal volunteer were acquired with a Siemens Vision MR scanner using breath-hold segmented k-space imaging sequences. Eight parallel short-axis slices were obtained orthogonal to the central axis of the LV spaced 11.5 mm apart, together with six long-axis slices oriented 30° apart about the LV central axis. Each slice was 8 mm thick and comprised 19 frames through the cardiac cycle. The image resolution ranged from 1.17 to 1.37 mm/pixel, depending on the field of view.

2.8. Simulated deformation

Simulated images were also generated of a prescribed deformation, in order to validate the method and determine whether errors are introduced in the calculation of model tags and model stripe points or in the search for image stripe centroids. The deformation was prescribed to mimic the displacements seen in the normal LV. An initial regular ED geometry was constructed in prolate spheroidal coordinates (f = 42 mm), with inner surface at λ = 0.60 and outer surface at λ = 0.85. The final ES geometry had an inner surface at λ = 0.40 and outer surface at λ = 0.82, with a longitudinal contraction of 15% in μ and uniform twist in θ from 24° and 21° at the endocardial and epicardial apex respectively to −8° and −7° at the endocardial and epicardial base respectively. The prolate model was converted to rectangular Cartesian coordinates (Figure 5) and model tags (8 mm apart) were calculated for eight short-axis images spaced 10 mm apart and six long-axis images spaced 30°
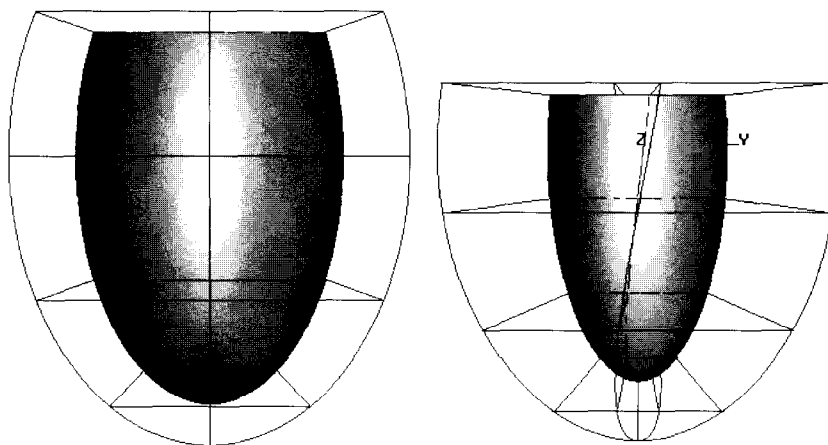
Figure 5. Prescribed (simulated) model deformation. Left, ED; right, ES. The inner surface is shaded and lines denote element boundaries.
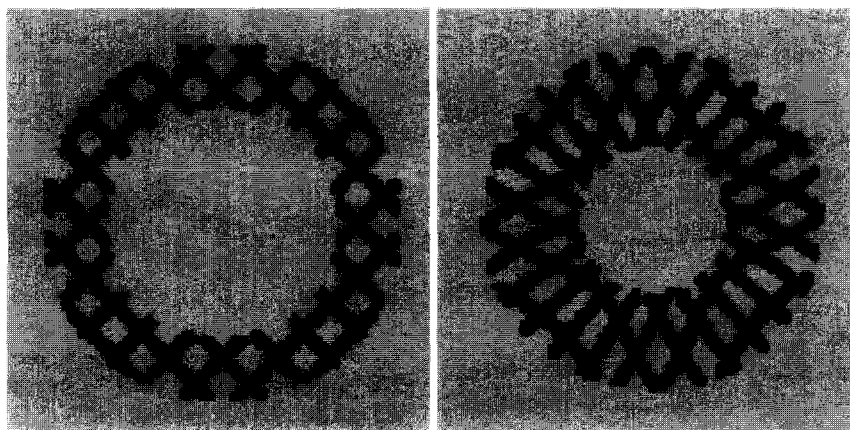

Figure 6. Simulated images from the prescribed deformation. ED (left) and ES (right) images from a short-axis slice.

apart about the central axis. The number and placement of the image and tag planes were chosen to mimic the typical case in clinical imaging.

Simulated images were then calculated at a resolution of 1.17 mm/pixel by assigning each pixel within the inner and outer boundaries to a representative myocardial grey level and each pixel within 1 mm of a model stripe point to a representative stripe grey level. Figure 6 shows resulting ED and ES images from a short-axis slice.

The simulated images were also analysed using a previously described stripe-tracking and model-fitting procedure (Young *et al.*, 1995). Briefly, the stripes were tracked in each slice using an active contour model of the 2-D tagging grid. The finite-element model was then used to reconstruct the 3-D displacements of material points by fitting the motion

from ES to ED. Then the ED model was deformed to ES by fitting the reconstructed 3-D displacements of the stripe data. This method has been validated using a gel phantom which was constrained to undergo 3-D deformations for which exact solutions could be derived analytically (Young *et al.*, 1995).

3. RESULTS

3.1. Initial geometry
In total 103 guide points were required for the ED geometry of the normal volunteer (53 for the endocardial surface and 50 for the epicardial surface). As there were 14 image slices this represents 3–4 points/surface/slice. Figure 7 shows the final ED geometry together with the associated guide points.
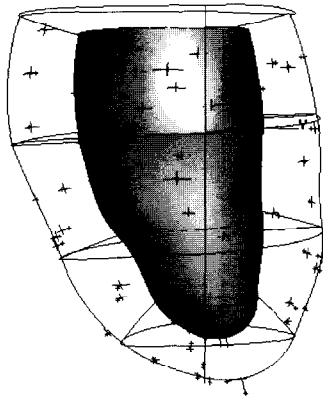
Figure 7. Model fit to guide points at ED. Endocardial surface shaded, guide data shown as '+'. Corresponding model locations (joined to each guide point with a line) are shown with cross-hairs.

The geometry in the third frame was determined first, then the guide points were moved to match the motion of the stripes back to the ED frame. The process required <10 min to complete, compared with ~45 min to manually define each boundary on each slice individually and then fit the ED geometry.

3.2. Model deformation

Using the tag plane positions and orientations derived from the imaging parameters, 182 model tags were found within the ED geometry. The model was then deformed to each frame by fitting the location of the model stripe points to the image stripes. A small motion occurred between the tag creation and the time of the ED image, so this frame was also fitted in the same manner. The deformed ED geometry was then used as the prior (undeformed state) in the smoothing term (Equation (5) for all subsequent frames. Figure 8 shows three of the model tags (two from the short-axis images and one from a long-axis image) at tag creation and ES.

Figure 9 shows short- and long-axis images at ES with model stripe points overlayed. Typically, one guide iteration (~30 guide points) and two image iterations (~4900 points) per frame were sufficient to achieve good correspondence between image stripes and model stripe points.

The 3-D tracking procedure took ~5 min per frame, representing a considerable time saving over the previous method (Young et al., 1995) which required definition of the inner and outer boundaries and image stripe tracking for each frame followed by 3-D model fitting (~45 min/frame). Each iteration (least-squares fit) took ~30 s to compute on a
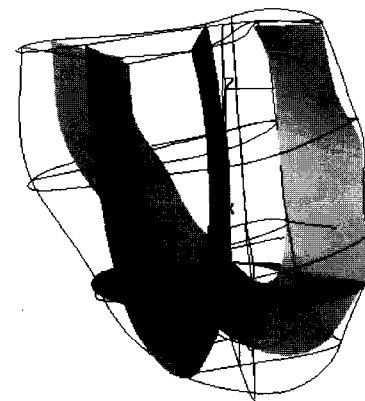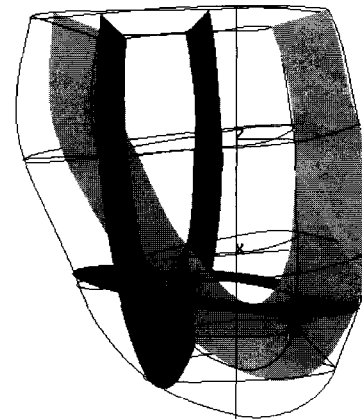

Figure 8. Model tags at the time of creation (left) and at ES (right). The two lighter tags are from the short-axis images, while the dark tag is from a long-axis image.

180 MHz R5000 workstation, however the code has not been optimized for execution speed.

3.3. Simulated deformation

The simulated ED geometry was deformed to fit the simulated image stripes in the same manner as above. Typically, two guide points per frame were required to bring the model into approximate correspondence. The root-mean-squared (RMS) errors in the displacement were 0.38 mm in x, 0.34 mm in y and 0.34 mm in z (the image pixel size was 1.17 mm). RMS errors in Lagrangian strain were 0.022 in circumferential strain (true range -0.357 to 0.088), 0.021 in longitudinal strain (true range -0.350 to -0.117) and 0.187 for radial strain (true range 0.446–0.930).

These images were also analysed using a previously described 2-D stripe tracking algorithm and 3-D finite-element model-fitting technique. The RMS errors of the
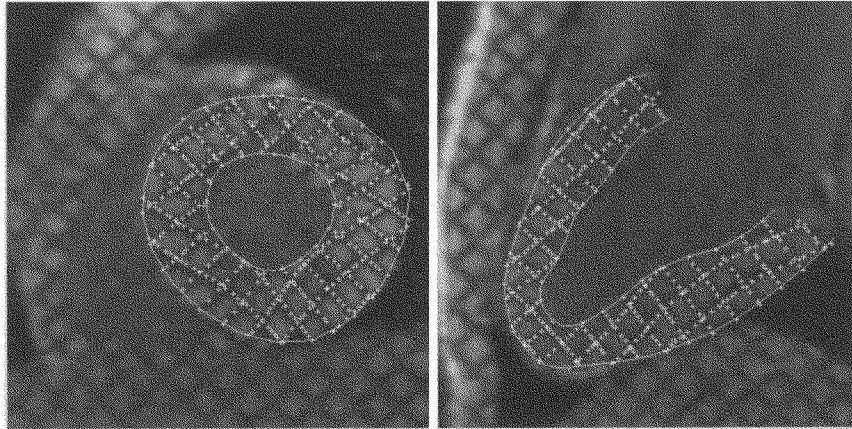
Figure 9. Short- (left) and long- (right) axis images at ES with model stripe points overlayed.

resulting displacement were 0.29 mm in x, 0.38 mm in y and 0.38 mm in z. Strain estimates had RMS errors of 0.023 in circumferential strain, 0.020 in longitudinal strain and 0.186 in radial strain. Thus the direct 3-D tracking method resulted in similar errors to the 2-D tracking/3-D fitting method. The error was greatest in the radial (transmural) direction and was mainly due to the lack of tag resolution in this direction, especially at the apex where there was only one stripe orthogonal to the radial direction.

4. DISCUSSION

This paper describes a method for directly reconstructing the shape and motion of the LV from short- and long-axis tagged MR images. The use of a 3-D model to track the stripes implicitly constrained the motion in each slice to be compatible with its 3-D neighbours. Thus, all stripes in all images contributed to the tracking process in a coherent 3-D manner, reducing the tracking errors which can arise from individual image analysis. User interaction was also constrained to act on the 3-D model, thereby maintaining compatibility between displacements and reducing the amount of interaction. Novel features of the method were: (i) the use of very sparse guide points in combination with model smoothing to approximate the geometry at ED and provide a user interface to correct for tracking errors; (ii) the calculation of model tags as material surfaces of arbitrary orientation within the model; and (iii) precalculation of the image displacement constraints, reducing the search for corresponding image stripe points to a simple look-up operation.

Previously, the 3-D reconstruction of LV motion from tagged MR images has required the prior identification of the inner and outer boundaries of the heart together with the

location of the image stripes. Young et al. (1995) described a tracking procedure in which the stripes were tracked separately for each slice using an active contour model of the 2-D tagging grid. The 3-D motion of material points was then reconstructed by fitting a finite-element model to the tracked stripe data. The FE model and objective function were similar to the present method; however, the minimization is now an iterative procedure because the location of the element (material) coordinates of the image stripe points are not known a priori. This increase in computational complexity is offset by the reduced user interaction and the simultaneous tracking of all image slices.

Park et al. (1996a, b) developed a class of deformable model with parametric global deformations which varied locally to capture the heart motion. The deformation functions governed twist, radial and longitudinal deformation, and model parameters were fitted to a priori contour and stripe data. Rather than model the tag surfaces, tag planes were assumed to translate without bending in the through-plane direction from frame to frame. Boundary points were included in the deformation analysis to compensate for the lack of tag data resolution in the transmural direction. Boundary edge information could easily be added to the direct 3-D tracking method described above; however, the edge information is obscured by the tagging saturation pulses, the variable blood grey level and the presence of the papillary muscles. The addition of boundary data would therefore require increased user interaction.

O'Donnell et al. (1995, 1996) described a deformable model with both global and local components of motion. Deformation parameters were fitted to a priori contour and stripe data. Global deformation parameters were not used in the current 3-D tracking method; rather, guide

points were used to obtain an approximate deformation before image data were applied. A model-based smoothing constraint [Equation (5)] was used to penalize the variation of deformation around the model and interpolate the very sparse guide data. This allowed a globally smooth deformation to be produced interactively in an intuitive manner without the need to separate global from local deformations.

Denney (1997) described a stripe-tracking procedure which did not require prior knowledge of the inner and outer contours of the heart. An active contour model was used to track stripes across an entire region of interest and a maximum *a posteriori* (MAP) hypothesis test was used to segment myocardial tag stripes from background. Such contour-free stripe data could be used as input to model-free motion reconstruction methods such as the method developed by Denney and McVeigh (1997), or that of Kerwin and Prince (1997). These methods do not require the prior formation of a geometric model; however, regional analyses of material strains require further processing. One advantage of a model-based approach is that the same model can be used to evaluate regional strain or deformation parameters, using the model to register corresponding regions between patients.

Radeva *et al.* (1997) developed a *B*-spline tensor product 3-D model (a '*B*-solid') to describe the deformation of the LV. The parameters were fitted directly to the stripes in short-axis images using a snake-type algorithm. The method could be used to reconstruct 3-D motion by including parallel long-axis images, provided that all tag planes correspond to isoparametric surfaces in the *B*-solid. This approach is very similar to the present work in that a 3-D model is fitted directly to image data. We have used a heart-based model to describe the LV geometry and deformation since this provides a natural representation of both the geometry and the deformation, whereas the tag-based model of Radeva *et al.* (1997) must embed a separate description of the LV surfaces into the cuboid space described by the *B*-solid. Also, the FE models fitted using the present technique can be directly used in more complex FE analyses of stress and activation (Costa *et al.*, 1996). Finally, no restriction is placed on the placement or orientation of the tag planes in the heart, since tags or images from the long-axis series generally are not orthogonal to the short-axis tags or images.

The direct 3-D tracking method was applied to images simulated from a known deformation for the FE model. The purpose of this experiment was to determine whether errors are introduced in the calculation of model tags and model stripe points or in the search for image stripe centroids. The accuracy of displacement and strain estimation was similar to that of a previously validated stripe-tracking and fitting method, suggesting that these errors are due to the stripe data density and distribution rather than to methodological errors.

A number of model and imaging parameters could effect the errors obtained. These include the number of elements, type of basis functions and the degree and type of smoothing [Equation (5)] used in the model, the number of images in each series and tag spacing, the number of model stripe points included in the fit and the design of the filters used to find the corresponding image stripe points. The optimum values of many of these parameters will depend on the disease processes occurring in the patients themselves, since heart motion is very dependent on the underlying pathology. Also, image quality generally degrades with the health of the patient, due to difficulty in maintaining a breath-hold and increased heart rate variability. A comprehensive error analysis must therefore await more data on cardiac motion in diseased states.

In conclusion, the 3-D tracking method improves the clinical utility of 3-D tagged cardiac images by decreasing the time required for analysis. User interaction was minimized since each guide constraint acted directly on the 3-D model and could influence a number of images at once. This represents a substantial time saving over methods which track stripes in each slice separately. Further improvements to the algorithm, including more efficient solution schemes and hierarchical refinement of model complexity, should allow real-time interaction, thereby increasing its utility in the clinical environment.

REFERENCES

Axel, L. and Dougherty, L. (1989) Heart wall motion: improved method of spatial modulation of magnetization for MR imaging. *Radiology*, 172, 349–350.

Costa, K. D., Hunter, P. J., Rogers, J. M., Guccione, J. M., Waldman, L. K. and McCulloch, A. D. (1996) A three-dimensional finite-element method for large elastic deformations of ventricular myocardium: part 1—cylindrical and spherical polar coordinates. *ASME J. Biomech. Eng.*, 118, 452–463.

Davatzikos, C. A. and Prince, J. L. (1995) An active contour model for mapping the cortex. *IEEE Trans. Med. Imag.*, 14, 65–80.

Davatzikos, C. A. and Prince, J. L. (1996) Convexity analysis of active contour problems. In *Proc. Computer Vision and Pattern Recognition*. IEEE Press, New York.

Declerck, J., Ayache, A. and McVeigh, E. M. (1998) Use of a 4D planispheric transformation for the tracking and the analysis of LV motion with tagged MR images. *INRIA Technical Report #3535*, France.

Denney, T. S. Jr (1997) Identification of myocardial tags in tagged MR images without prior knowledge of myocardial contours. In *XVth Int. Conf. on Information Processing in Medical Imaging*, pp. 327–340. CRC Press, New York.

Denney, T. S. Jr and McVeigh, E. R. (1997) Model-free reconstruction of three-dimensional myocardial strain from planar tagged MR images. *J. Magn. Reson. Imag.*, 7, 799–810.

Guttman, M. A., Prince, J. L. and McVeigh, E. R. (1994) Tag and contour detection in tagged MR images of the left ventricle. *IEEE Trans. Med. Imag.*, 13, 74–88.

Hildreth, E. C. (1984) Computations underlying the measurement of visual motion. *Artif. Intell.*, 23, 309–354.

Kerwin, W. S. and Prince, J. L. (1997) Generating 3D cardiac material markers using tagged MRI. In *XVth Int. Conf. on Information Processing in Medical Imaging*, pp. 313–326. CRC Press, New York.

Kraitchman, D. L., Young, A. A., Chang, C.-N. and Axel, L. (1995) Semi-automatic tracking of myocardial motion in MR tagged images. *IEEE Trans. Med. Imag.*, 14, 422–433.

Lorensen, W. E. and Cline, H. E. (1987) Marching cubes: a high resolution 3D surface construction algorithm. *Comp. Graphics.*, 21, 163–169.

Marquardt, D. W. (1963) An algorithm for least squares estimation of non-linear parameters. *J. Soc. Indust. Appl. Math.*, 11, 431–441.

O'Dell, W. G., Moore, C. C., Hunter, W. C., Zerhouni, E. A. and McVeigh, E. R. (1995) Three-dimensional myocardial deformations: calculation with displacement field fitting to tagged MR images. *Radiology*, 195, 829–835.

O'Donnell, T., Gupta, A. and Boult, T. (1995) The hybrid volumetric ventriculoid: new model for MR-SPAMM 3-D analysis. In *Proc. Computers in Cardiology*, pp. 5–8. CRC Press, New York.

O'Donnell, T., Boult, T. and Gupta, A. (1996) Global models with parametric offsets as applied to cardiac motion recovery. In *Proc. Computer Vision and Pattern Recognition*, pp. 293–299. IEEE Press, New York.

Palmon, L. C., Reichek, N., Yeon, S. B., Clark, N. R., Brownson, D., Hoffman, E. and Axel, L. (1994) Intramural myocardial shortening in hypertensive left ventricular hypertrophy with normal pump function. *Circulation*, 89, 122–131.

Park, J., Metaxas, D., Young, A. A. and Axel, L. (1996a) Deformable models with parameter functions for cardiac motion analysis from tagged MRI data. *IEEE Trans. Med. Imag.*, 15, 278–289.

Park, J., Metaxas, D. and Axel, L. (1996b) Analysis of left ventricular wall motion based on volumetric deformable models and MRI-SPAMM. *Med. Image Anal.*, 1, 53–71.

Radeva, P., Amini, A. A. and Huang, J. (1997) Deformable B-solids and implicit snakes for 3D localization and tracking of SPAMM MRI data. *Comp. Vision Image Understanding*, 66, 163–178.

Terzopoulos, D. (1988) The computation of visible-surface representations. *IEEE Trans. PAMI*, 10, 417–438.

Young, A. A., Axel, L., Dougherty, L., Bogen, D. K. and Parenteau, C. S. (1993) Validation of tagging with MRI to estimate material deformation. *Radiology*, 188, 101–108.

Young, A. A., Kramer, C. M., Ferrari, V. A., Axel, L. and Reichek, N. (1994) Three-dimensional left ventricular deformation in hypertrophic cardiomyopathy. *Circulation*, 90, 854–867.

Young, A. A., Kraitchman, D. L., Dougherty, L. and Axel, L. (1995) Tracking and finite-element analysis of stripe deformation in magnetic resonance tagging. *IEEE Trans. Med. Imag.*, 14, 413–421.

Young, A. A., Fayad, Z. A. and Axel, L. (1996) Right ventricular midwall surface motion and deformation using magnetic resonance tagging. *Am. J. Physiol.*, 271, H2677–H2688.

Zerhouni, E. A., Parish, D. M., Rogers, W. J., Yang, A. and Shapiro, E. P. (1988) Human heart: tagging with MR imaging—a method for non-invasive assessment of myocardial motion. *Radiology*, 169, 59–63.

APPENDIX. MINIMIZATION ALGORITHM

A Levenburg–Marquardt algorithm (Marquardt, 1963) was used to minimize Equation (4), as had been done previously for RV surface models (Young *et al.*, 1996). Gaussian quadrature was used to calculate the integrals in Equation (5), allowing both smoothing, guide and image data constraints to be expressed in terms of sums of squares. The objective function Equation (4) can then be written as

$$E = \left\| \mathbf{Sq} \right\|^2 + \left\| \mathbf{Jq} - \mathbf{p} \right\|^2 \qquad (A1)$$

where $\mathbf{S}$ is a matrix containing derivatives of the deformation gradient tensor at the Gauss points, $\mathbf{J}$ is a matrix containing model basis functions evaluated at ξ_j and weighted by the tag normals, $\mathbf{p}$ is a vector containing components of $\mathbf{x}_j$ weighted by the tag normals and $\mathbf{q}$ is a vector of model parameters. Note that $\mathbf{J}$ varies with $\mathbf{q}$, but $\mathbf{S}$ does not.

The Newton method minimizes E by neglecting terms higher than second order in the Taylor series expansion, giving the following iteration:

$$\mathbf{H}_k(\mathbf{q}_{k+1} - \mathbf{q}_k) = -\left. \frac{\partial E}{\partial \mathbf{q}} \right|_k \qquad (A2)$$

where $\mathbf{H}$ is the Hessian matrix of second derivatives of E. The right-hand side of Equation (A2) has a component due to the fact that ξ_j can change with $\mathbf{q}$. However, the error function Equation (4) measures the squared distance from each data point to the model position ξ_j in the direction approximately perpendicular to the model tag surface. Since ξ_j can only change within the model tag surface, the contribution to the first derivative of the error function due to changes in model position will be small. We therefore use the linear approximation

$$\frac{\partial E}{\partial \mathbf{q}} = \mathbf{S}^T \mathbf{Sq} + \mathbf{J}^T \mathbf{Jq} - \mathbf{J}^T \mathbf{p}. \qquad (A3)$$

Replacing the Hessian H with the linear approximation $S^T S + J^T J$, and adding a term ΛI ($\Lambda \geq 0$) to avoid non-positive definite H, gives the iteration

$$(S^T S + J_k^T J_k + \Lambda I)\mathbf{q}_{k+1} = \Lambda I + J_k^T \mathbf{p}. \qquad (A4)$$

If Λ is large the step becomes small and in the direction of steepest descent; if Λ is small the update becomes a full Gauss–Newton step. In practice, all the iterations were performed with $\Lambda = 0$, equivalent to solving the linear problem that arises if the ξ_j are assumed to be constant over the step.